First observation of CO at 345 GHz in the atmosphere of Saturn with the JCMT. New constaints on its origin

T. Cavalié, F. Billebaud, M. Dobrijevic, T. Fouchet, E. Lellouch, T. Encrenaz, J. Brillet, P. Moriarty, J.P. Wouterloot, P. Hartogh

▶ **To cite this version:**

HAL Id: hal-00400419
https://hal.archives-ouvertes.fr/hal-00400419

Submitted on 30 Jun 2009

First observation of CO at 345 GHz in the atmosphere of Saturn with the JCMT. New constraints on its origin.

T. Cavalié [a,*] , F. Billebaud [b,c], M. Dobrijevic [b,c], T. Fouchet [d], E. Lellouch [d], T. Encrenaz [d], J. Brillet [b,c], G. H. Moriarty-Schieven [e], J. G. A. Wouterloot [f], P. Hartogh [a]

[a] *Max Planck Institute for Solar System Research, 37191 Katlenburg-Lindau, Germany*

[b] *Université de Bordeaux, Laboratoire d'Astrophysique de Bordeaux (LAB), France*

[c] *CNRS/INSU, UMR 5804, 33271 Floirac cedex, France*

[d] *LESIA, Observatoire de Paris, 92195 Meudon, France*

[e] *National Research Council, Herzberg Institute of Astrophysics, Victoria, BC V9E 2E7, Canada*

[f] *Joint Astronomy Center, Hilo, 96720 Hawaii, USA*

Abstract

We have performed the first observation of the CO(3-2) spectral line in the atmosphere of Saturn with the James Clerk Maxwell Telescope. We have used a transport model of the atmosphere of Saturn to constrain the origin of the observed CO. The CO line is best fitted when the CO is located at pressures lower than ~15 mbar implying an external origin. This favors an origin due to a comet impact ~200-300 years ago rather than to continuous deposition by interplanetary dust particles (IDP) or local sources (rings/satellites). This result tends to confirm that comet impacts are periodic and efficient providers of CO to the atmospheres of the outer planets. Finally, we have tentatively derived an upper limit of $\sim 0.5 \times 10^{-9}$ on the tropospheric CO mixing ratio.

Key words: Saturn, atmosphere, spectroscopy

* Tel: +49-5556-979-541; fax: +49-5556-979-240
  Email address: `cavalie@mps.mpg.de` (T. Cavalié).

1   Introduction

Infrared observations conducted with the Infrared Space Observatory and more recently with Spitzer have led to the detection of water vapor and carbon dioxide in the atmospheres of the outer planets and Titan (Feuchtgruber et al., 1997, 1999; Coustenis et al., 1998; Burgdorf et al., 2006). These detections have raised the question of the origin of the oxygen compounds present above the tropospheric cold trap in the reducing atmospheres of the outer planets. Eligible external sources are of three different kinds: local (rings and satellites), diffuse (interplanetary dust particles) and sporadic sources (large comet impacts). While the comet supply seems to prevail in the atmosphere of Jupiter as shown by infrared (ISO) and submillimeter (SWAS and Odin) observations (Lellouch et al., 2002; Cavalié et al., 2008a), local sources could be the major external supplier of water to the atmosphere of Saturn (Prangé et al., 2006).

As for carbon monoxide, it has been detected in the atmospheres of all giant planets by Beer (1975), Noll et al. (1986), Encrenaz et al. (2004) and Marten et al. (1993). Addressing the question of the origin of CO in the atmospheres of the outer planets is more complex than it is for H_2O. Indeed, CO does not condense at the tropopause level in any of the atmospheres of the giant planets. Thus, an additional source is likely to provide CO to the upper atmosphere in a significant way by means of upwards convective mixing originating from the deep hot atmosphere. Giant planet formation models (Lissauer (1993) and Lissauer (2005), for example) predict that oxygen compounds are abundant in the planets' deep hot interiors. Convection transports these species upwards of the atmosphere. Being in thermochemical disequilibrium, CO is converted to CH_4 and H_2O. The tropospheric mixing ratio of CO is finally fixed at the altitude at which the chemical reaction timescale equals the convective transport characteristic time. Thus, measuring the tropospheric abundance of CO constrains the internal source strength. Upon an assumption on the eddy diffusion coefficient value at this so-called "quench" level, this measurement provides a constraint on the deep O/H ratio by giving the deep water abundance (Bézard et al., 2002).

Recent studies of infrared, millimeter and submillimeter spectra of Jupiter and Neptune have shown that CO has a dual origin (internal and external) in both atmospheres (Bézard et al., 2002; Lellouch et al., 2005; Hesman et al., 2007). In Jupiter, a 1 ppb tropospheric CO mixing ratio (hereafter q_{CO}) of internal origin has been observed, resulting in a O/H ratio of 0.6-9 times the solar value. On the other hand, a value of 0.5 ppm has been measured in the troposphere of Neptune. Such a high q_{CO} value implies an enhancement of the O/H ratio of 440 times the solar value (Lodders and Fegley, 1994) or the inhibition of the conversion reaction between CO and CH_4. In both atmospheres,

an additional, external source of CO is observed. It is characterized by an increasing mixing ratio with altitude in the stratosphere. Measurements of the CO/H_2O deposition rate by an external supply have led to values as large as 20 and possibly larger than 200 (Lellouch et al., 2005). Such values seem to be inconsistent with an oxygen supply by interplanetary dust particles, thus favoring a cometary origin.

Infrared observations of Saturn and Uranus have led to the detection of CO (Noll et al., 1986; Encrenaz et al., 2004). In the case of Saturn, the spectral resolution in the latest published observations of CO (Noll and Larson, 1991) was not sufficient to distinguish between an internal and an external origin of CO. More recently, millimeter observations have only led to the derival of upper limits on the CO mixing ratio (Rosenqvist et al., 1992; Cavalié et al., 2008b). This is the reason why we have carried out new observations of Saturn. We chose to perform them at a higher frequency than the ones of our last attempt (Cavalié et al., 2008b) because models predict that the CO lines should be stronger (Cavalié et al., 2007). In this paper, we present the detection of CO in the atmosphere of Saturn from submillimeter spectroscopy. The observation of the CO(3-2) line has been analysed in order to constrain the internal and external sources of CO.

2   Observations and data reduction

We used the 15-m James Clerk Maxwell Telescope (Mauna Kea, Hawaii, USA) to observe the CO(3-2) line at 345.796 GHz. We used this telescope to observe Saturn on 14-15 January 2008 (UT). The angular size of the planet was 19.4 arcsec×17.6 arcsec with a ring inclination angle of 7°.

Observations have been carried out at the frequency of the CO(3-2) line with HARP, a 16-receptor heterodyne array receiver (Smith et al., 2008). Two contiguous receptors beeing separated by 30 arcsec, we chose to observe Saturn in a balanced position-switching mode with the ON position centered on the H10 receiver and the OFF position centered on the H08 receiver at 60 arcsec from the ON position. Such a choice enabled us to use both H10 and H08 receivers of the array simultaneously. The zenith opacity of the atmosphere at 225 GHz was 0.08 and 0.06 the first and second night respectively, resulting in system temperatures ranging from 320 to 450 K (H10, 1st night), from 390 to 440 K (H08, 1st night), from 260 to 340 K (H10, 2nd night) and from 310 to 340 K (H08, 2nd night).

At 345 GHz, the atmospheric levels sounded are located between 10 mbar and 1 bar. CO lines can be very broad when formed at such pressures. This is the reason why we have recorded the spectrum of Saturn over a wide range
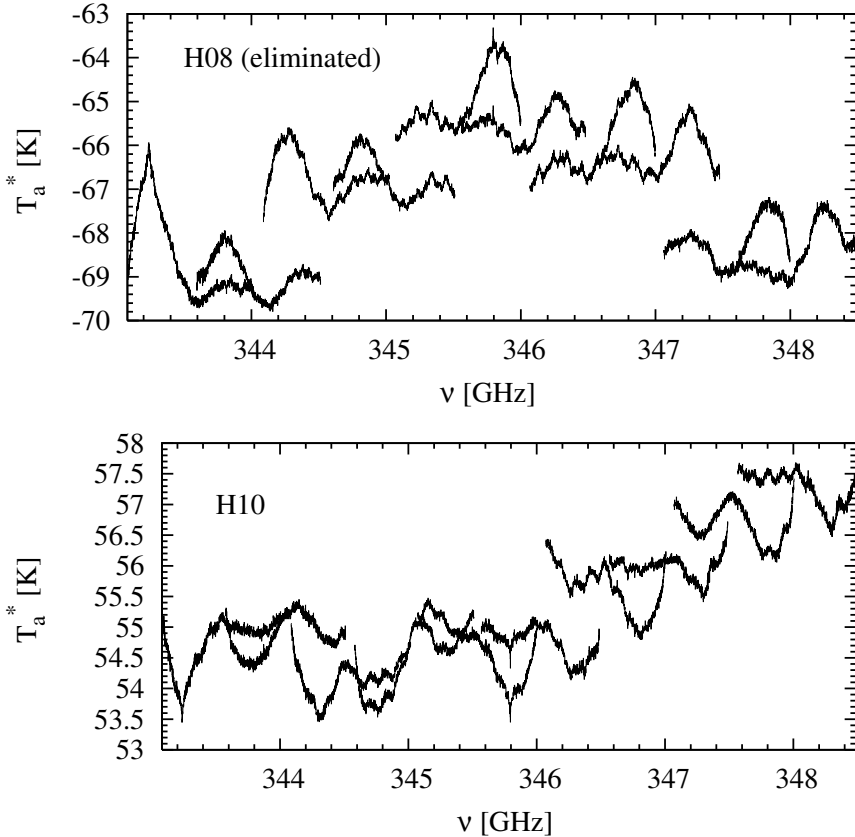
Fig. 1. Observed spectrum of Saturn at 345 GHz with the H08 receptor and the H10 receptor. The CO line is detected in the two central sub-bands of the H10 receptor observations (in absorption) and in one of those of the H08 receptor observations (in emission). The H08 spectrum appears with negative T_a^* values because the H08 pixel was our OFF position pixel. This spectrum has not been used in the data reduction because of the irregular shape of the ripple. The deep absorption feature which is seen at 343.2 GHz is the O_3 terrestrial line.

of frequencies. Because the ACSIS spectrometer enables observations in several bandwidth/spectral resolution modes, we chose to observe simultaneously 2 sub-bands of 1 GHz with a spectral resolution of 1 MHz in a single-side band mode. The bandwidth of each observed sub-band being 1 GHz, we have observed 10 contiguous bands with 50% overlaps between 2 contiguous bands. The central frequencies of the tunings which have been selected start at 343.545 GHz and end at 348.045 GHz, thus covering 5.5 GHz. The observations on H10 and H08 are shown in Fig. 1. The different continuum level seen with the H08 and H10 receptors cannot be explained by pointing errors and we regard this difference as being due to an instrumental effect. Besides, observations of Mars have been carried out simultaneously in order to obtain an absolute measurement of Saturn's brightness temperature at 345 GHz. So, this difference, which is also seen on the Mars observations, has no effect on our results.
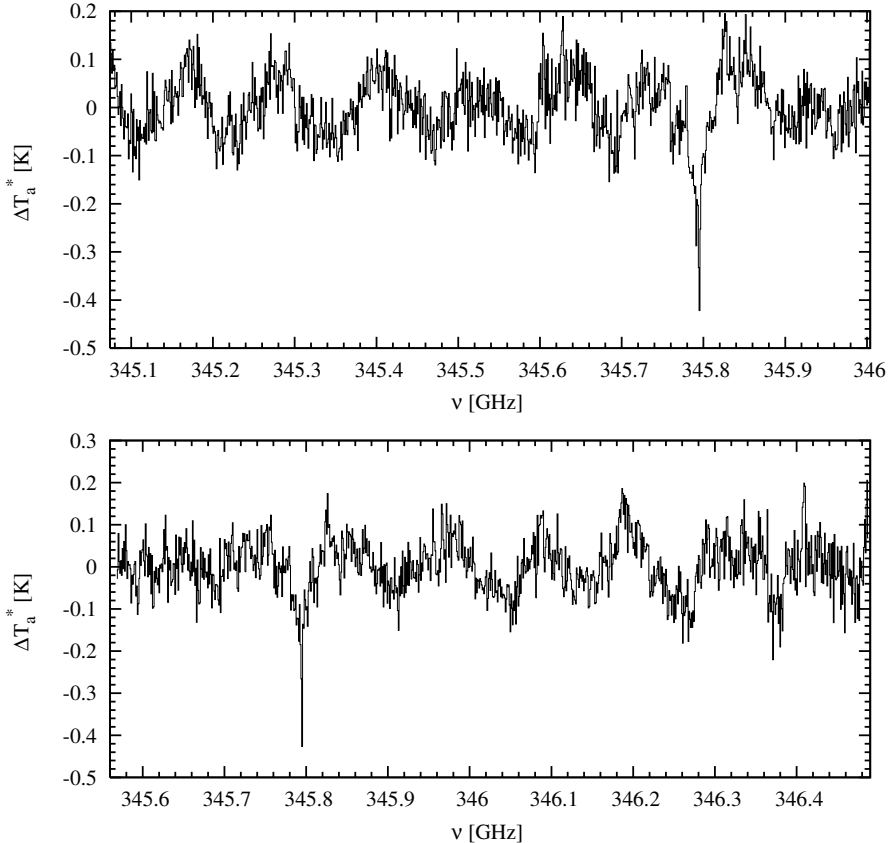
Fig. 2. Central sub-bands showing the CO line as well as the strongest ripple. Because this ripple is observed in each sub-band and has a regular shape, it has been removed from each sub-band before connecting and averaging them.

We note that the CO line was independently detected in three out of the four central sub-bands (two with the H10 receptor and one with the H08 receptor). As we targeted a faint CO line, we reduced each sub-band before connecting and averaging them. The first step of the data reduction consisted in removing a polynomial baseline. We then removed a ripple, which period is about 100 MHz (see Fig. 2 for example), with a FFT procedure since it was present in each sub-band. Because the ripple has a period which has the same order of magnitude as the line width, the ripple removal adds some uncertainty in the final width of the observed line. This ripple had an irregular shape in the H08 spectra, so the data from this receptor were not included in our final analysis. The last stage of the data reduction consisted in connecting the sub-bands by rescaling them one to another. The fact that we had 50% overlap between 2 contiguous sub-bands resulted in doubling the integration time at all frequencies and hence in lowering the noise level when averaging them. To increase the signal-to-noise ratio, the final spectrum was smoothed to a resolution of 16 MHz.

Table 1
Observational parameters used in the computation of Saturn's brightness temperature at 345 GHz.

	(T_a^*)	FF
Mars	63±5 K	2.02
Saturn	54±5 K	1.45

Notes. The parameter FF is the beam filling factor of the antenna.

3 The brightness temperature of Saturn at 345 GHz

Observations of Mars have been performed at 345 GHz in order to measure Saturn's brightness temperature $(T_b)_{\mathrm{Saturn}}$. The angular size of Mars was 14.2 arcsec. The values we have used to compute Saturn's brightness temperature at 345 GHz are given in Table 2. Following Griffin et al. (1986), the brightness temperature of Mars at the time of the observations can be obtained by interpolating logarithmically the brightness temperature of Mars at 350 μm and 3.3 mm. Observations at 350 μm yield a brightness temperature of $(T_b)_{\mathrm{Mars}}$=(210±7) K (Wright, 1976). At 3.3 mm, the brightness temperature given by Ulich (1981) is $(T_b)_{\mathrm{Mars}}$=(202±6) K. Thus, we obtain $(T_b)_{\mathrm{Mars}}$=(206±7) K at 345 GHz. Finally, the brightness temperature of Saturn at 345 GHz is:

$$(T_b)_{\mathrm{Saturn}} = (127 \pm 26) \text{ K}. \tag{1}$$

We have also used the Lellouch and Amri model[1] as a second way of computing the brightness temperature of Mars. This model uses the surface and sub-surface temperatures taken from the Mars Climate Database (Lewis et al., 1999; Forget et al., 2006) and the ephemerides from the IMCCE[2] to compute the thermal emission of Mars. This model yields $(T_b)_{\mathrm{Mars}}$=213.2 K at 345 GHz at the time of the observations. So the value for Saturn is in that case:

$$(T_b)_{\mathrm{Saturn}} = (131 \pm 23) \text{ K}. \tag{2}$$

We have used the radiative transfer model described in Cavalié et al. (2008b) to compute the spectrum of Saturn in the frequency range of the CO(3-2) line. The primary beam size at 345 GHz is 14.3 arcsec, so we have used a disk-averaged temperature profile (Ollivier et al., 2000). The opacity of the continuum at millimeter wavelengths is mainly due to H_2-He-CH_4 collision-induced absorption (Borysow et al., 1985; Borysow and Frommhold, 1986; Borysow et al., 1988). We have also included the opacity due to NH_3 and

---

[1] *http://www.lesia.obspm.fr/∼lellouch/mars*
[2] *http://www.imcce.fr*

6

PH$_3$ lines to model the continuum in the observed frequency range. The spectroscopic parameters which have been used in our computations are given in Table 2 of Cavalié et al. (2008b). Our computations lead to a disk-averaged brightness temperature of 135 K. At the time of the observations, the ring inclination was 7°, so the ring shadowing and the ring emission have to be taken into account. Following (and extrapolating the results of) de Pater and Dickel (1991), Dunn et al. (2005) and Melnick et al. (1983), we assume a ring brightness temperature of 40±15 K at 345 GHz and an optical depth of 0.8±0.4 for the A and B rings. By using the formalism of Melnick et al. (1983), we find that the rings absorb more than they emit at 345 GHz. The brightness temperature of the Saturn+rings system we model is thus 123±4 K.

This result fits well the brightness temperature derived from the observations and from the use of Mars brightness temperatures at 3.3 mm and 350 μm (see eq. 1). It is also within the error bars of the brightness temperature derived from the observations and from the use of Lellouch and Amri's thermal model of Mars (see eq. 2), but there is a greater difference with the nominal value (difference of 8 K). The thermal emission of Mars is certainly better modelled by Lellouch and Amri's model than from the interpolation of the brightness temperature of Mars at 3.3 mm and 350 μm. So, we believe that the difference between the observations and our modelling is due to our poor knowledge of the brightness temperature and of the optical depth of the rings at 345 GHz. In that sense, interferometric observations would be very valuable in order to obtain these values for the Saturn+rings system at submillimeter wavelengths. In what follows, the spectra generated by our model are rescaled to the Lellouch and Amri continuum value and are interpreted in terms of line-to-continuum ratio.

4   New constraints on the origin of CO in the atmosphere of Saturn

The main result of these observations is the first observation of a CO millimeter/submillimeter line. In the spectrum of Saturn, the CO(3-2) rotational line is detected with a peak-to-continuum signal-to-noise ratio of $\sim$7. Because the detected line probes the high troposphere/low stratosphere, we can constrain the CO mixing ratio vertical profile in the 10 mbar-1 bar pressure levels. In a first step, this section presents fits obtained with simple vertical profiles. These profiles are either uniform with altitude (internal origin only for CO) or constant above a given pressure level which is located above the tropopause (external origin only for CO). In a second step, we have constrained the value of the CO continuous external flux which is required to reproduce the observed spectral feature from vertical transport modelling. Finally, we consider the hypothesis of a supply of oxygen material being due to a (sub-)kilometer sized comet impact.
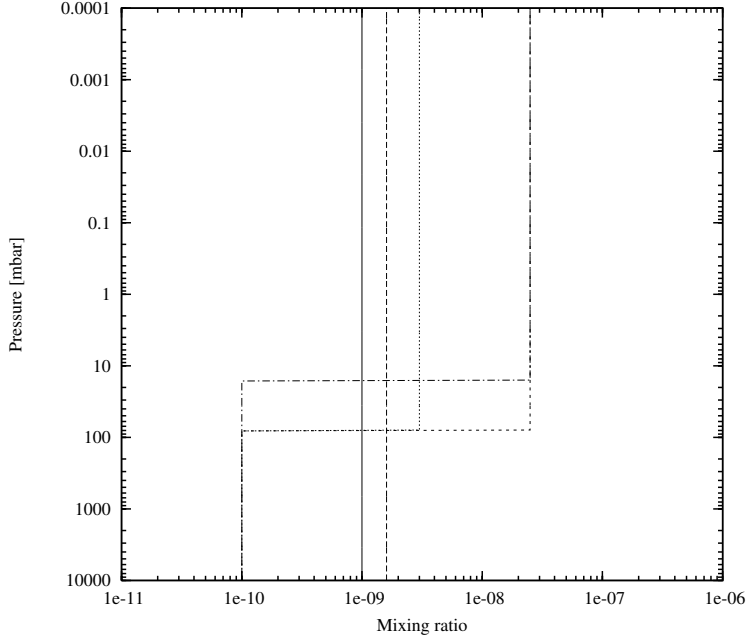
Fig. 3. Original and modified CO mixing ratio vertical profiles used in the modelling presented in Section 4.1. Solid line: $q_{CO}=10^{-9}$, uniform with altitude (Noll and Larson, 1991); Long-dashed lines: $q_{CO}=1.6\times10^{-9}$ (Bézard et al., 1989); Short-dashed lines: $q_{CO}=1\times10^{-10}$ if $p > 80$ mbar and $q_{CO}=2.5\times10^{-8}$ if $p \leq 80$ mbar (Noll and Larson, 1991); Dotted lines: $q_{CO}=1\times10^{-10}$ if $p > 80$ mbar and $q_{CO}=3\times10^{-9}$ if $p \leq 80$ mbar; Dashed-dotted lines: $q_{CO}=1\times10^{-10}$ if $p > \sim15$ mbar and $q_{CO}=2.5\times10^{-8}$ if $p \leq \sim15$ mbar (best fit model).

4.1 Initial guesses on the CO vertical profile

In a first approach, we have modelled the observed CO line with simplified CO mixing ratio vertical profiles. The profiles are shown in Fig. 3.

In the case of an internal origin hypothesis, the CO originates from the deep hot layers of the troposphere. Its observable mixing ratio is fixed at an altitude where the convective transport characteristic time equals the chemical timescale of the conversion of CO to CH_4. Above this so-called "quench" level, the conversion of CO is inhibited by vertical transport so that the mole fraction of CO remains constant with altitude. Past observations of CO in the infrared have led to its detection (Noll and Larson, 1991). But, from modelling the observed spectra, the author could not distinguish a model for which the CO has an internal origin only, with $q_{CO}=10^{-9}$ uniformly mixed with altitude, from a model in which CO has an external origin only, with q_{CO} set to 2.5×10^{-8} above the tropopause. Modelling the observed CO(3-2) line with a constant vertical profile with 1 ppb of CO leads to the spectrum shown in Fig. 4. The obtained synthetic spectrum obviously underestimates the CO line strength. The best fit of the line depth is obtained by taking the CO mixing ratio in-
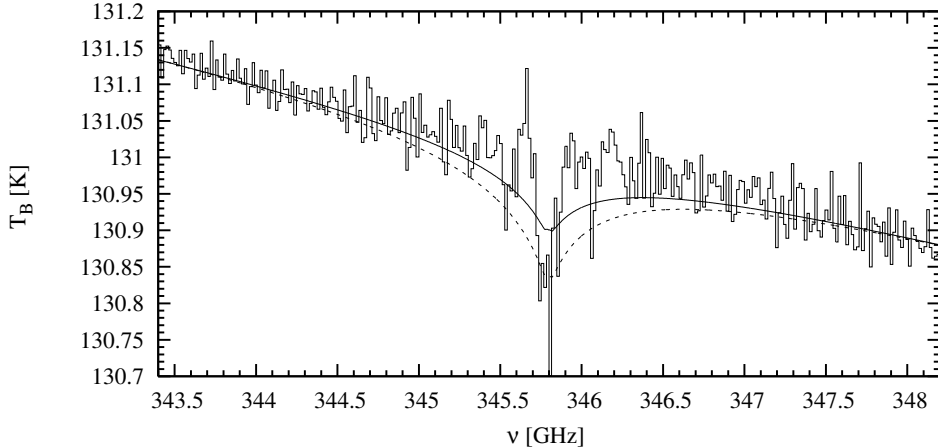
Fig. 4. Spectrum of Saturn at 345 GHz modelled with internal source only. The solid line corresponds to 1 ppb of CO uniformly mixed with altitude (Noll and Larson, 1991) and the dashed lines to 1.6 ppb of CO uniformly mixed with altitude (Bézard et al., 1989). The peak absorption pixel (right to 345.8 GHz) is due to the terrestrial mesospheric CO. This pixel of the spectrum is not reliable.

ferred from the infrared observations led by Bézard et al. (1989), which is $q_{CO}=1.6\times10^{-9}$. However, the width of the synthetic line is ~5 times greater than the observed linewidth. So the synthetic spectrum does not lie within the 3-σ uncertainty error bars of the observed spectrum. With regard to this result, a model for which CO has an internal origin only can be discarded, but it does not mean that a dual origin is ruled out. This specific point will be discussed in Section 4.3.

When considering only an external origin, Noll and Larson (1991) retrieved a mixing ratio of 2.5×10^{-8} above the tropopause (located at the 80 mbar pressure level). Fig. 5 shows the line computed from such a vertical profile. In this case, the computed absorption is much too deep. This implies either that the CO mixing ratio is lower above 80 mbar or that the CO cut-off level lies at a higher altitude in the stratosphere. Fig. 6 shows the best fit models obtained by either adjusting the CO mixing ratio above the cut-off level of 80 mbar or adjusting the cut-off level and keeping the CO mixing ratio fixed at 2.5×10^{-8}. Keeping the cut-off level at 80 mbar implies lowering the CO mixing ratio to a value of 3×10^{-9} above this level. The resulting line is too broad, whereas a much better fit is obtained when translating the cut-off level at ~15 mbar and keeping the CO mixing ratio at its initial value of 2.5×10^{-8}. So a model with a CO mixing ratio of 2.5×10^{-8} at pressures lower than ~15 mbar and a CO mixing ratio between 10^{-10} and 10^{-9} at higher pressures could model both the infrared observations and this observation (see Sect. 4.3 for a discussion on the internal source of CO in the atmosphere of Saturn).

The first outcomes of this work are that modelling the observations with simplified vertical profiles rules out those models in which CO only has an internal
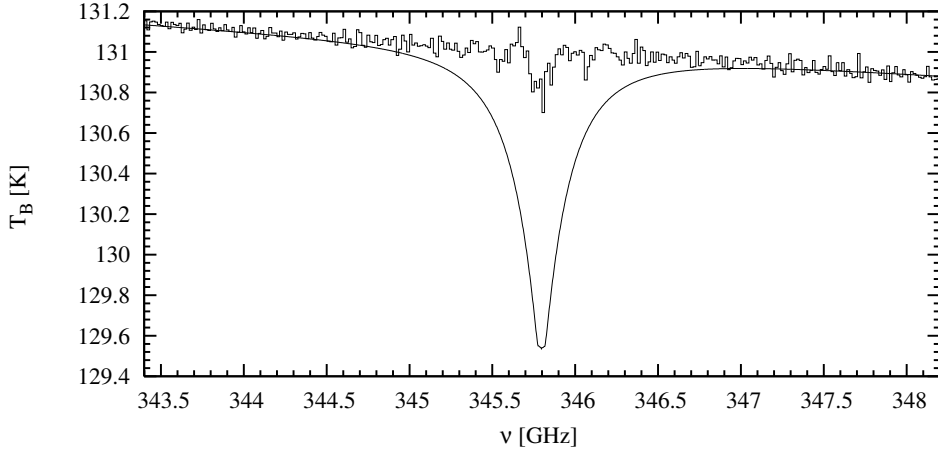
Fig. 5. Spectrum of Saturn at 345 GHz modelled with a CO vertical profile where 25 ppb of CO are restricted to the stratosphere ($p <$80 mbar).
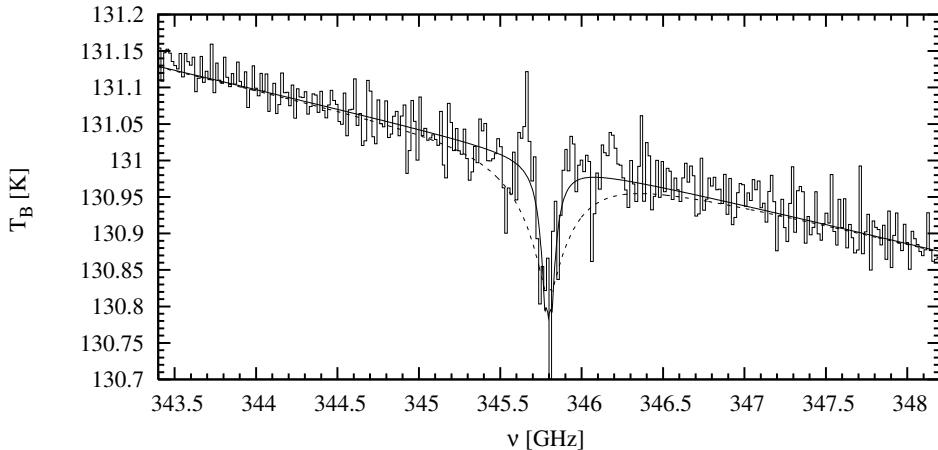

Fig. 6. Spectrum of Saturn at 345 GHz modelled with vertical profiles where 25 ppb of CO are restricted to levels where $p <\sim$15 mbar (solid line) or where 3 ppb of CO are uniformly mixed above the tropopause ($p <$80 mbar) (dashed lines).

origin and indicates that CO seems to be restricted to the stratosphere at pressures lower than $\sim$15 mbar with a mixing ratio of 2.5×10^{-8}.

4.2 External source of CO

Because the signal-to-noise ratio of our observation is low, we chose to model the CO vertical profile with no more than two variables. The variables can be either a CO permanent flux or a CO deposit and its deposition time due to a comet impact. So, we chose not to take photochemistry into account but only transport. Doing this way, we neglect the oxygen compound chemistry. However, CO is a stable molecule and H_2O photochemistry only adds small amounts of CO. We used a 1D time-dependent transport model of the at-
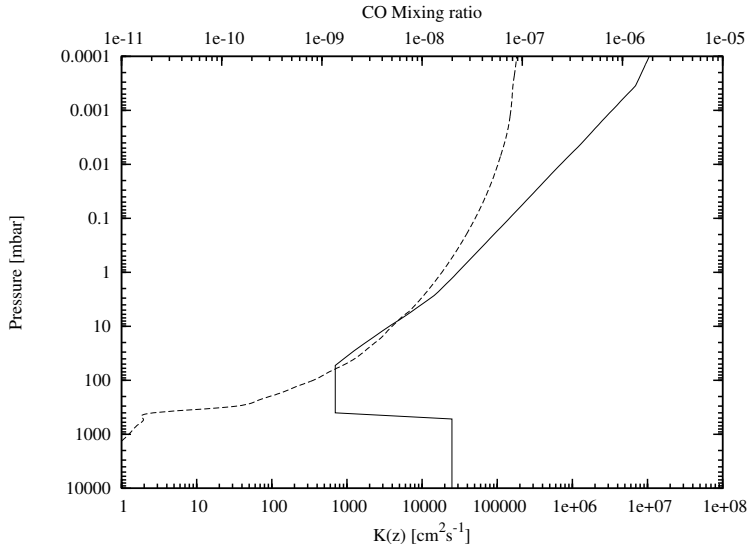
Fig. 7. Eddy diffusion coefficient vertical profile adopted in the vertical transport model (solid line). The CO mixing ratio vertical profile which gives the best agreement to the observations is obtained with a permanent and uniform CO flux of 1.5×10^6 cm^{-2}·s^{-1} (dashed lines).

mosphere of Saturn to test the external source hypothesis by generating CO mixing ratio vertical profiles. This model is described in the next subsection. Then, we will present the results obtained using this transport model.

4.2.1 Transport model

Our transport model is taken from the photochemical model of Saturn's atmosphere developed by Ollivier et al. (2000). The diffusion equation

$$\frac{dy_{CO}}{dt} = -\frac{1}{n}\text{div}(\phi_{CO}.\vec{e_z}) \tag{3}$$

is solved with a semi-explicit Crank-Nicholson scheme. In this equation, y_{CO} is the molar fraction of CO, n the atmospheric concentration, ϕ_{CO} the flux of CO and $\vec{e_z}$ is a unit vector in the direction z. This flux accounts for molecular and eddy diffusion. The eddy diffusion coefficient profile $K(z)$ (in cm^2·s^{-1}) we have adopted is shown in Fig. 7. It comes from Moses et al. (2000a) for the stratosphere and from Edgington et al. (1997) for the troposphere.

The lower and upper boundaries of the model are located respectively at -250 km (16.6×10^3 mbar) and 2500 km (7.7×10^{-8} mbar). At the lower boundary, the internal source of CO can be controlled via the value of the CO molar fraction, which is here fixed at 0 because we aim at deriving the strength of an external source of CO. At the upper boundary, the external source is represented by a infalling flux of CO.

11

In the following subsections, we will investigate two kinds of supply of CO to the atmosphere of Saturn using both this transport model and our radiative transfer model. First, we will retrieve the CO flux corresponding to the case of a continuous supply (IDP, rings, satellites). And then, we will consider the possibility of a sporadic supply (large comet).

4.2.2 The diffuse and/or local source hypothesis

In this section, we have supposed that all the CO is deposited in the upper part of the atmosphere of Saturn by a permanent and uniform external source and that the CO molecules are subsequently transported to higher pressure levels by eddy mixing. This model encompasses the hypotheses of a local (rings, satellites) and of a diffuse source (IDP). Indeed, the planet was not spatially resolved during our observations. So, we cannot distinguish a local supply from a uniform supply.

The best fit is obtained with a flux of CO of ϕ_{CO}=1.5×10^6 cm^{-2}·s^{-1}. The resulting vertical profile is shown in Fig. 7 and the resulting spectrum is plotted in Fig. 8. The width of the line, as computed from this model, is ∼3 times larger than the width of the observed line. Such a broadening comes from the fact that, due to transport, CO reaches levels which are too deep in the atmosphere of Saturn. Besides, Moses et al. (2000b) derived a H_2O external flux of 0.5-2×10^6 cm^{-2}·s^{-1} from the ISO dataset analysis. In their nominal model, their H_2O flux is 1.5×10^6 cm^{-2}·s^{-1}. Ollivier et al. (2000) derived a similar result (ϕ_{H_2O}=1.0×10^6 cm^{-2}·s^{-1}). If we compare these values to the CO flux we obtain from our modelling, then the H_2O:CO ratio is ∼1. This value seems to be incompatible with the relative composition of oxygen compounds of interstellar and cometary ice as inferred by Despois (1997); Bockelée-Morvan et al. (2000). Indeed, the H_2O:CO ratio in interstellar and cometary ice is ∼5. On the other hand, such a low H_2O:CO ratio is compatible with a deposit of oxygen compounds during a comet impact, as H_2O is mostly converted into CO during comet impacts. Finally, from the width of the modelled line and from the value of the CO flux we derive, a continuous source for CO seems to be unlikely, contrary to the case of H_2O (Ollivier et al., 2000; Moses et al., 2000b; Prangé et al., 2006).

4.2.3 The (sub-)kilometer-sized comet impact hypothesis

Recent results obtained from CO observations at infrared and (sub-)millimeter wavelengths have shown that significant amounts of oxygen compounds can be carried into outer planet atmospheres at the submillibar level by comet impacts. From their infrared high spectral resolution observations, Bézard et al. (2002) have shown that CO is regularly supplied to the atmosphere
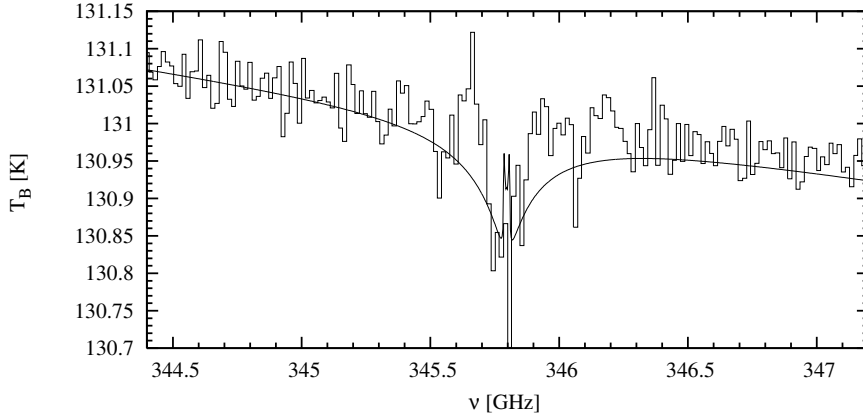
Fig. 8. The best fit model in the case of a diffuse and/or local source is provided with a CO external continuous flux of 1.5×10^6 cm$^{-2} \cdot$s^{-1}.

of Jupiter by large comet impacts, the last example being the Shoemaker-Levy 9 (SL9) impacts in July 1994. During the SL9 impacts, a total mass of $6.0 \pm 4.0 \times 10^{14}$ g of CO was deposited (Moreno et al., 2003). The periodicity of SL9-like impacts at Jupiter has been estimated in several works. Generally, this periodicity ranges from 200 to 5000 years (Roulston and Ahrens, 1997; Bézard et al., 2002; Zahnle et al., 2003). In the atmosphere of Neptune, Lellouch et al. (2005) and Hesman et al. (2007) have found that the CO mixing ratio increases with the altitude. The flux derived from their (sub-)millimeter observations implies that the ratio of the CO and H_2O deposition rates is as large as 10 to 500. From this result, the authors conclude that the CO has been delivered to the atmosphere of Neptune by a comet impact 200 years ago. However, Lellouch et al. (2005) and Hesman et al. (2007) give discrepant value of the comet size (2 km and 10 km, respectively).

At Saturn, comet impact rates are lower than at Jupiter only by a factor of $\sim$3 (Levison et al., 2000). So, the probability for the observed stratospheric CO to be originating from a comet impact is still not negligible. Moreover, the vertical profile shape we have obtained in a first attempt (see Sect. 4.1) is very similar to the first guess vertical profile in Lellouch et al. (2005). In the atmosphere of Neptune, they find $p_0 = 20$ mbar and we obtain $p_0 \sim 15$ mbar in the atmosphere of Saturn. If the observed CO was deposited by a comet impact at 0.1 mbar as in the case of Jupiter and SL9, then the diffusion time Δt down to 15 mbar is given by:

$$\Delta t = \int_{z'}^{z''} \frac{H(z)dz}{K(z) + D_{\mathrm{CO}}(z)} \simeq 350 \text{ years} \qquad (4)$$

where z' and z'' are the altitudes at which the pressure are 0.1 mbar and 15 mbar respectively, H the atmospheric scale height, K the eddy diffusion coefficient and D_{CO} the molecular diffusion coefficient for CO. The CO flux
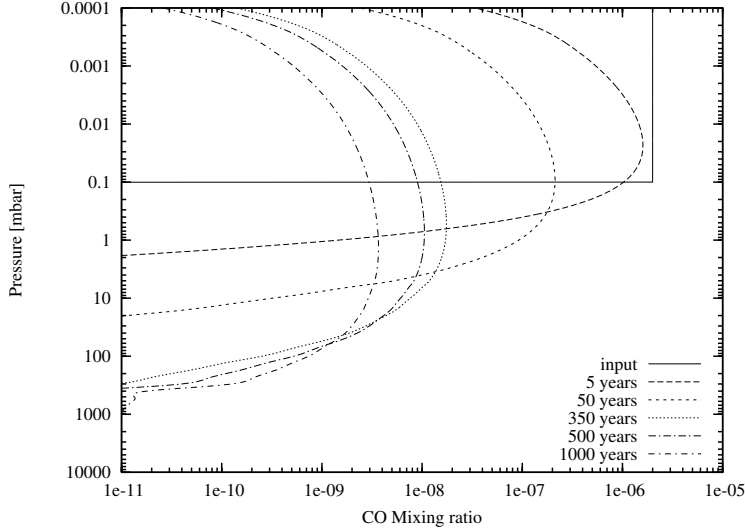
13

Fig. 9. Evolution in time of the CO mixing ratio vertical profile after a cometary input of $q_{CO}=2\times10^{-6}$ above 0.1 mbar. Different curves show the profile at the time of the impact and then 5, 50, 350, 500 and 1000 years later.

needed to model the observations, which is given by our transport computations, is $\sim1.5\times10^{6}$ cm^{-2}·s^{-1}. If integrated over 350 years and over the surface of the planet, such a flux yields 7.5×10^{36} CO molecules. This corresponds to 3.3×10^{14} g of CO. If the density of the comet is ~0.5 g.cm^{-3} (Asphaug and Benz, 1996) and if CO represents $\sim50\%$ of the delivered mass (Crovisier, 1996), then the size of the comet is ~1.1 km. This is approximately the size of an SL9-like comet (Moreno et al., 2003).

With regard to the values (diffusion time, comet mass) determined above, a cometary origin for CO can be considered. In order to test the cometary source hypothesis, we have computed CO mixing ratio vertical profiles in the same manner as in Cavalié et al. (2008a) with the transport model described previously. In our modelling, the CO is uniformly deposited [3] in the atmosphere above 0.1 mbar by a comet impact at a time t_0 and the permanent CO external flux is set to 0 cm^{-2}·s^{-1}. Then, we use our time-dependent transport model to compute the vertical profiles at $t > t_0$. Examples of CO vertical profiles obtained 5, 50, 350, 500 and 1000 years after an impact, characterized by an initial input of $q_{CO}=2\times10^{-6}$ above 0.1 mbar, are shown in Fig. 9.

There are two parameters that can be adjusted (impact date and initial CO mixing ratio) by fitting the observation. If we take the result of Eq. (4) as the time elapsed after the comet impact, then the best match is obtained with an initial mixing ratio of 2×10^{-6}. The CO vertical profile 350 years after the

---

[3] Refer to Cavalié et al. (2008a) for a justification of the validity of such an hypothesis (uniform deposition of the oxygen material) in the case of spatially unresolved observations of the planet.
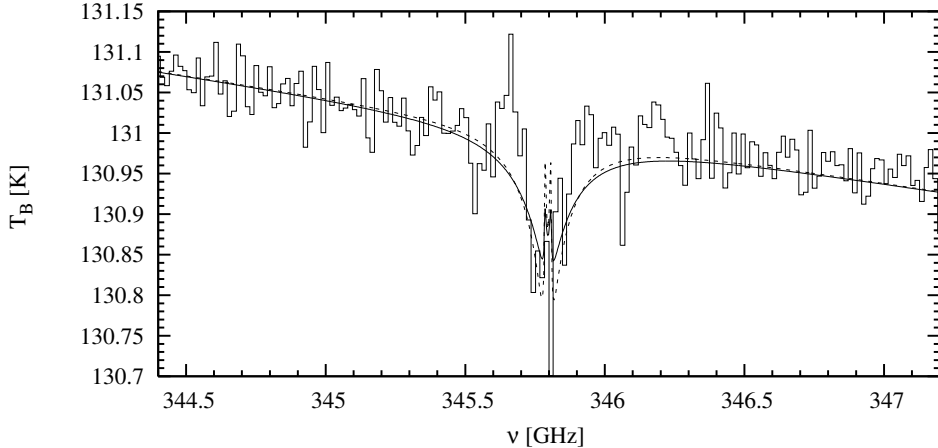
Fig. 10. The best fit model in the case of a cometary supply of CO 350 years ago is obtained with $q_{CO}=2\times10^{-6}$ above 0.1 mbar (solid line). Another good agreement is obtained in the case of a cometary supply of CO 200 years ago with $q_{CO}=4\times10^{-6}$ above 0.1 mbar (dashed lines).

impact is shown in Fig. 9 and the fit to the observations in Fig. 10. The value of q_{CO} is consistent with the value inferred in the case of the SL9 CO supply to Jupiter (Bézard et al., 2002). Increasing the time elapsed after the impact implies increasing the value of q_{CO}. It results in a broader line which is not satisfactory. On the other hand, decreasing the time elapsed after the impact and increasing the initially deposited mixing ratio of CO is a way of having a slightly narrower line. It also results in a stronger emission line core. The example with $t_0=200$ years and an initial mixing ratio of 4×10^{-6} is shown in Fig. 10. If we take a shorter time, then we get a line in emission with too faint an absorption feature. So the range of values for t_0 and q_{CO} are approximately 200-350 years and 2-4×10^{-6} respectively.

As impact chemistry favors the conversion of H_2O into CO, $\sim90\%$ of the supplied oxygen would come in the form of CO and only $\sim10\%$ in the form of H_2O (Zahnle, 1996). Because a sporadic supply of H_2O is quickly (~14 years) removed by condensation in the atmosphere of Saturn (Moses et al., 2000b), CO would quickly remain the only signature (in terms of the presence of oxygen material) of a cometary impact in the atmosphere of Saturn. So, it is not inconsistent to model the oxygen input of a comet with CO only. In the end, we regard the impact of an SL9-like comet ~200-300 years ago as being the most likely source of CO in the atmosphere of Saturn. For H_2O, however, the case is different as it is probably supplied by a continuous source (like IDP or rings) (Prangé et al., 2006).
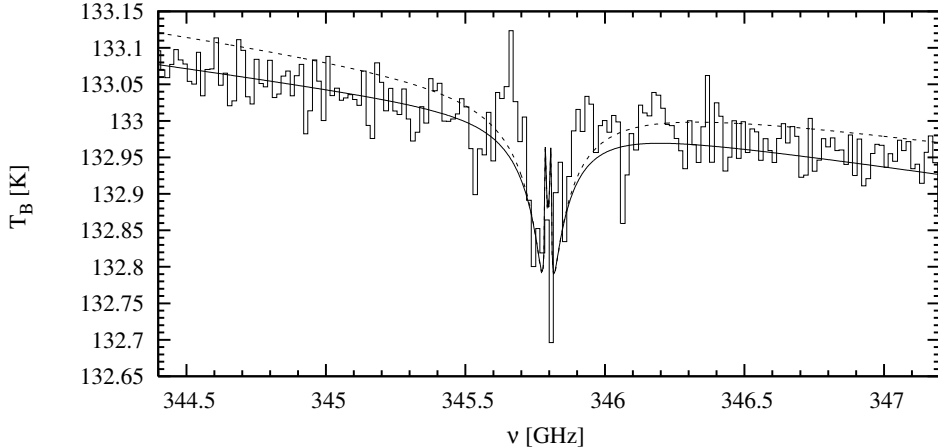
15

Fig. 11. Comet impact model (with t_0=200 years and q_{CO}=4×10^{-6}) with an internal source of 5×10^{-10} (dashed lines) and without no internal source (solid line). The value of 5×10^{-10} corresponds to the upper limit fixed on a possible CO internal component filtered out by our data reduction procedure.

4.3   Internal source of CO

4.3.1   Upper limit on the internal source

An internal source is not included in our best fit models, but it does not mean that an internal component is not present. Indeed, the ripple removal process leads to an uncertainty on the width and strength of the line (see Sect. 2). It could have resulted in filtering out the signature of an internal component. Such a component would be characterised by a very broad absorption feature, as shown in Fig. 4 (models with a CO internal source only). The real line would then be slightly stronger and slightly broader. Because it is hazardous to try to estimate the uncertainty on the internal component strength from the line after the removal of the ripple, we tentatively put an upper limit of ~5×10^{-10} on q_{CO} in the troposphere, corresponding to the 3-σ noise level of our spectrum. The comparison between the comet impact model (with t_0=200 years and q_{CO}=4×10^{-6}) and the same model with the addition of an internal component of 5×10^{-10} can be seen in Fig. 11. This upper limit remains uncertain and requires confirmation by new observations, either in the (sub)millimeter range or in the infrared range (with high spectral resolution).

4.3.2   Implications on the O/H ratio in Saturn's deep atmosphere

The CO mixing ratio in the troposphere of the giant planets is proportionnal to the deep H_2O mixing ratio and thus to the internal O/H ratio (Fegley and Prinn, 1988; Lodders and Fegley, 1994) and is fixed at the "quench" level. The "quench" level corresponds to the level where the chemical lifetime of

CO (τ_{chem}) equals its convective diffusion timescale (τ_{mix}). Its temperature thus depends on the CO destruction chemical scheme. In these schemes, the chemical timescale is governed by the rate-limiting reaction where the C=O bond is broken. Prinn and Barshay (1977) initially proposed this reaction to be $H_2CO+H_2\rightarrow CH_3+OH$. Later, Yung et al. (1988) proposed a two-step reaction scheme in which the rate-limiting reaction is $H+H_2CO+M\rightarrow CH_3O+M$. Visscher and Fegley (2005) have computed the temperature at the CO "quench" level in the atmosphere of Saturn in both cases. The values they have retrieved are 1036 K for the chemical scheme of Prinn and Barshay (1977) and 922 K for the one of Yung et al. (1988). In both cases, the eddy mixing coefficient has been set to $\sim 10^9$ cm$^2\cdot$s^{-1}.

In their Eq. (8), Visscher and Fegley (2005) have written the direct link between the CO mixing ratio and the O/H elemental ratio enrichment of Saturn over the solar value as a function of the "quench" level temperature. One has to note that this equation does not depend on the CO destruction chemical scheme. Thus, we have used this equation to compute the possible ranges of O/H ratio enrichment factors as a function of the observable CO tropospheric mixing ratio, by setting the "quench" temperature at the values given by both chemical schemes and setting the CH_4 enrichment to 7.4 (Flasar et al., 2005; Fletcher et al., 2009). The results are shown in Fig. 12.

Our upper limit on the tropospheric value of q_{CO} results in upper limits on the O/H ratio enrichment factor. Indeed, if the one-step chemical scheme of Prinn and Barshay (1977) reflects the way CO is destroyed, then the O/H ratio enrichment factor is lower than 1.2. This upper limit is low when compared to N/H and C/H ratios in Jupiter and Saturn. Indeed, carbon and nitrogen are enriched by a factor of 2.9±0.5 and 3.6±0.8 respectively in Jupiter (Atreya et al., 1999). In Saturn, the enrichements of carbon and nitrogen are respectively 7.4±1.7 and 2.75±0.75 (Flasar et al., 2005; Fletcher et al., 2009; Hersant et al., 2008). On the other hand, if the correct CO destruction scheme is the two-step process of Yung et al. (1988), then the O/H ratio enrichment factor is lower than 13. This upper limit is in agreement with the range of values derived by Bézard et al. (2002) in the case of Jupiter (0.2-9). It is fully consistent with giant planet formation models where heavy elements are trapped in the amorphous ice of planetesimals (Owen et al., 1999; Owen and Encrenaz, 2006). It is also consistent with the hydrate clathration of heavy elements scenario proposed by Gautier and Hersant (2005) and Hersant et al. (2008), which requires a large O/H ratio enrichment (>10).

The large uncertainty on the chemical scheme which is responsible for the destruction of CO as well as the large error bars on the "quench" level temperature[4] (±100 K), as shown in Bézard et al. (2002), result in large error

---

[4] These error bars are due to error bars in the chemical rate of the rate-limiting
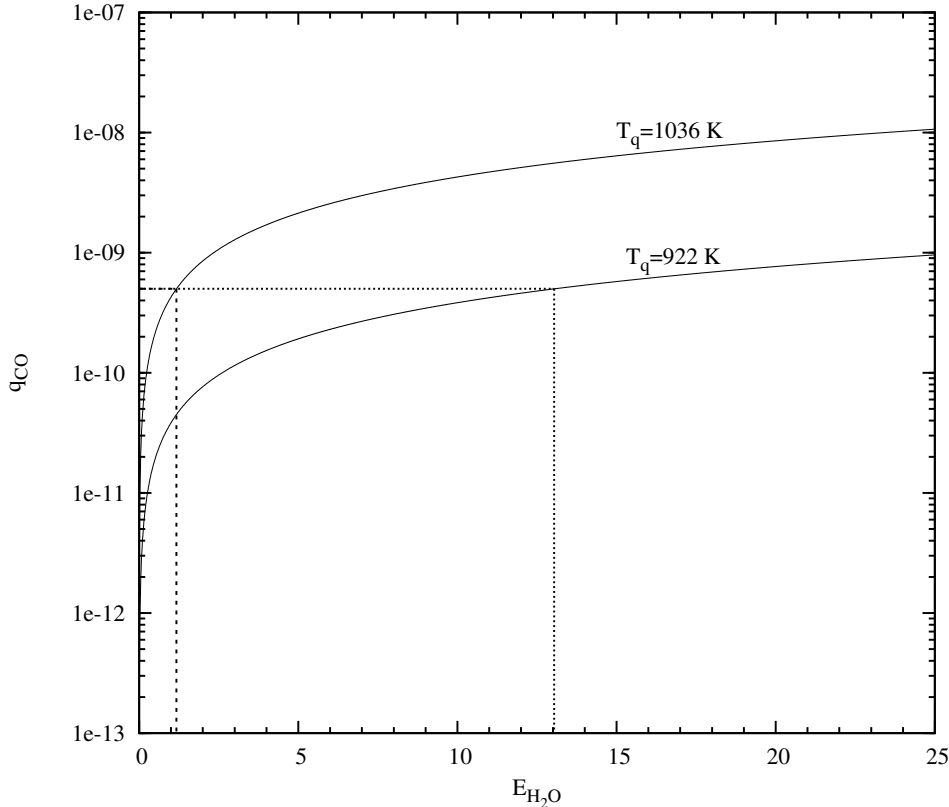
Fig. 12. Observable tropospheric CO mixing ratio (q_{CO}) as a function of the O/H ratio enrichment (E_{H_2O}) in the deep atmosphere of Saturn. Different curves correspond to different "quench" level temperatures. Each different "quench" level temperature corresponds to a different chemical scheme: 1036 K for the one-step process of Prinn and Barshay (1977) and 922 K for the two-step process of Yung et al. (1988).

bars on the O/H ratio enrichment. Moreover, the result also depends linearly on the accuracy of the CH_4 enrichment factor. Thus, it is not possible to conclude on the deep water abundance of Saturn and on its formation scenario. It would be very valuable to send a Galileo-like probe in the deep atmosphere of Saturn to directly measure the deep water abundance. Such a measurement would add a strong constraint on giant planet formation scenarios.

5   Summary and perspectives

We have performed observations of Saturn at submillimeter wavelengths with the James Clerk Maxwell Telescope. Our observations have led to the first observation of CO in the atmosphere of Saturn in the submillimeter range.

---

reaction.

We have detected the CO(3-2) line at 345 GHz with a multi-band observation method. Our subsequent modelling of the observed CO line with a transport model of the atmosphere of Saturn can be summarized as follows:

- The presence of CO at the levels which are probed by our observations (10-1000 mbar) cannot be attributed to an internal source. The observed CO line is due to an external supply of CO to the atmosphere of Saturn.
- The signature of an internal component may have been filtered out during the data reduction procedure (ripple subtraction). We tentatively put an upper limit on the tropospheric CO mixing ratio of 5×10^{-10}, based on the noise level in the continuum of the spectrum (see Fig. 11). This upper limit needs to be confirmed by new observations.
- Assuming a permanent and uniform external flux of CO, we retrieve a CO external flux of 1.5×10^6 cm^{-2}·s^{-1} (IDP or ring source) by modelling the transport in the atmosphere of Saturn. However, such a permanent flux does not give the best agreement with the data.
- The most likely source of CO to Saturn would be an SL9-like comet which impacted the planet $\sim$200-300 years ago. This tends to confirm that large comet impacts are important and regular providers of oxygen compounds into the atmospheres of the outer planets.

Even if the quality of our detection of CO is not sufficient to quantify a possible internal source of CO and to determine accurately the external source of CO in the atmosphere of Saturn, the modelling procedure we have developed will enable the derival of both quantities from future observations. The internal source could be constrained from new observations at submillimeter wavelengths when heterodyne broad-band spectrometers will become available. Besides, sending a probe in the atmosphere of Saturn to measure the deep water abundance as part of or in the end of the Titan Saturn System Mission (Coustenis et al., 2008) should be considered. It would provide a strong constraint to the processes which lead to the formation of the planet. In parallel, Herschel observations will enable the direct observation of CO at high stratospheric levels and thus permit the determination of the CO external source. More generally, observations of CO and H_2O with Herschel would be very valuable with respect to addressing the question of the origin of oxygen compounds.

References

Asphaug, E., Benz, W., 1996. Size, Density, and Structure of Comet Shoemaker-Levy 9 Inferred from the Physics of Tidal Breakup. Icarus 121, 225–248.

Atreya, S. K., Wong, M. H., Owen, T. C., Mahaffy, P. R., Niemann, H. B., de Pater, I., Drossart, P., Encrenaz, T., 1999. A comparison of the atmospheres of Jupiter and Saturn: deep atmospheric composition, cloud structure, vertical mixing, and origin. Planetary and Space Science 47, 1243–1262.

Beer, R., 1975. Detection of carbon monoxide in Jupiter. The Astrophysical Journal 200, L167–L169.

Bézard, B., Drossart, P., Lellouch, E., Tarrago, G., Maillard, J. P., 1989. Detection of arsine in Saturn. The Astrophysical Journal 346, 509–513.

Bézard, B., Lellouch, E., Strobel, D., Maillard, J.-P., Drossart, P., 2002. Carbon Monoxide on Jupiter: Evidence for Both Internal and External Sources. Icarus 159, 95–111.

Bockelée-Morvan, D., Lis, D. C., Wink, J. E., Despois, D., Crovisier, J., Bachiller, R., Benford, D. J., Biver, N., Colom, P., Davies, J. K., Gérard, E., Germain, B., Houde, M., Mehringer, D., Moreno, R., Paubert, G., Phillips, T. G., Rauer, H., 2000. New molecules found in comet C/1995 O1 (Hale-Bopp). Investigating the link between cometary and interstellar material. Astronomy and Astrophysics 353, 1101–1114.

Borysow, A., Frommhold, L., 1986. Theoretical collision-induced rototranslational absorption spectra for the outer planets - H2-CH4 pairs. The Astrophysical Journal 304, 849–865.

Borysow, J., Trafton, L., Frommhold, L., Birnbaum, G., 1985. Modeling of pressure-induced far-infrared absorption spectra Molecular hydrogen pairs. The Astrophysical Journal 296, 644–654.

Borysow, J., Frommhold, L., Birnbaum, G., 1988. Collison-induced rototranslational absorption spectra of H2-He pairs at temperatures from 40 to 3000 K. The Astrophysical Journal 326, 509–515.

Burgdorf, M., Orton, G., van Cleve, J., Meadows, V., Houck, J., 2006. Detection of new hydrocarbons in Uranus' atmosphere by infrared spectroscopy. Icarus 184, 634–637.

Cavalié, T., Billebaud, F., Lellouch, E., Fouchet, T., Dobrijevic, M., Encrenaz, T., Brillet, J., Herpin, F., 2007. CO in the stratospheres of Saturn, Uranus and Neptune seen with Herschel-HIFI. Herschel Open time Key Program Workshop, 20-21 Feb. 2007, ESTEC, Noordwick, The Netherlands.

Cavalié, T., Billebaud, F., Biver, N., Dobrijevic, M., Lellouch, E., Brillet, J., Lecacheux, A., Hjalmarson, A., Sandqvist, A., Frisk, U., Olberg, M., The Odin Team, Bergin, E. A., 2008a. Observation of water vapor in the

stratosphere of Jupiter with the Odin Space Telescope. Planetary and Space Science 56, 1573–1584.

Cavalié, T., Billebaud, F., Fouchet, T., Lellouch, E., Brillet, J., Dobrijevic, M., 2008b. Observations of CO on Saturn and Uranus at millimeter wavelengths: new upper limit determinations. Astronomy and Astrophysics 484, 555–561.

Coustenis, A., Salama, A., Lellouch, E., Encrenaz, T., Bjoraker, G. L., Samuelson, R. E., de Graauw, T., Feuchtgruber, H., Kessler, M. F., 1998. Evidence for water vapor in Titan's atmosphere from ISO/SWS data. Astronomy and Astrophysics 336, L85–L89.

Coustenis, A., and 155 colleagues, 2008. TandEM: Titan and Enceladus mission. Experimental Astronomy 23, 893–946.

Crovisier, J., 1996. Observational constraints on the composition and nature of Comet D/Shoemaker-Levy 9. In: Noll, K. S., Weaver, H. A., Feldman, P. D. (Eds.), IAU Colloq. 156: The Collision of Comet Shoemaker-Levy 9 and Jupiter. pp. 31–54.

de Pater, I., Dickel, J. R., 1991. Multifrequency radio observations of Saturn at ring inclination angles between 5 and 26 degrees. Icarus 94, 474–492.

Despois, D., 1997. Radio Line Observations Of Molecular And Isotopic Species In Comet C/1995 O1 (Hale-Bopp). Earth Moon and Planets 79, 103–124.

Dunn, D. E., de Pater, I., Wright, M., Hogerheijde, M. R., Molnar, L. A., 2005. High-Quality BIMA-OVRO Images of Saturn and its Rings at 1.3 and 3 Millimeters. The Astronomical Journal 129, 1109–1116.

Edgington, S. G., Atreya, S. K., Trafton, L. M., Caldwell, J. J., Beebe, R. F., Simon, A. A., West, R. A., Barnet, C., 1997. Phosphine Mixing Ratios and Eddy Mixing Coefficients in the Troposphere of Saturn. In: Bulletin of the American Astronomical Society. Vol. 29 of Bulletin of the American Astronomical Society. p. 992.

Encrenaz, T., Lellouch, E., Drossart, P., Feuchtgruber, H., Orton, G. S., Atreya, S. K., 2004. First detection of CO in Uranus. Astronomy and Astrophysics 413, L5–L9.

Fegley, B., Prinn, R. G., 1988. Chemical constraints on the water and total oxygen abundances in the deep atmosphere of Jupiter. The Astrophysical Journal 324, 621–625.

Feuchtgruber, H., Lellouch, E., de Graauw, T., Bezard, B., Encrenaz, T., Griffin, M., 1997. External supply of oxygen to the atmospheres of giant planets. Nature 389, 159–162.

Feuchtgruber, H., Lellouch, E., Encrenaz, T., Bezard, B., Coustenis, A., Drossart, P., Salama, A., de Graauw, T., Davis, G. R., 1999. Oxygen in the stratospheres of the giant planets and Titan. In: Cox, P., Kessler, M. (Eds.), The Universe as Seen by ISO. Vol. 427 of ESA Special Publication. p. 133.

Flasar, F. M., and 45 colleagues, 2005. Temperatures, Winds, and Composition in the Saturnian System. Science 307, 1247–1251.

Fletcher, L. N., Orton, G. S., Teanby, N. A., Irwin, P. G. J., Bjoraker, G. L., 2009. Methane and its isotopologues on Saturn from Cassini/CIRS obser-

vations. Icarus 199, 351–367.

Forget, F., Millour, E., Lebonnois, S., Montabone, L., Dassas, K., Lewis, S. R., Read, P. L., López-Valverde, M. A., González-Galindo, F., Montmessin, F., Lefèvre, F., Desjean, M.-C., Huot, J.-P., 2006. The new Mars climate database. In: Forget, F., Lopez-Valverde, M. A., Desjean, M. C., Huot, J. P., Lefevre, F., Lebonnois, S., Lewis, S. R., Millour, E., Read, P. L., Wilson, R. J. (Eds.), Mars Atmosphere Modelling and Observations. p. 128.

Gautier, D., Hersant, F., 2005. Formation and Composition of Planetesimals. Space Science Reviews 116, 25–52.

Griffin, M. J., Ade, P. A. R., Orton, G. S., Robson, E. I., Gear, W. K., Nolt, I. G., Radostitz, J. V., 1986. Submillimeter and millimeter observations of Jupiter. Icarus 65, 244–256.

Hersant, F., Gautier, D., Tobie, G., Lunine, J. I., 2008. Interpretation of the carbon abundance in Saturn measured by Cassini. Planetary and Space Science 56, 1103–1111.

Hesman, B. E., Davis, G. R., Matthews, H. E., Orton, G. S., 2007. The abundance profile of CO in Neptune's atmosphere. Icarus 186, 342–353.

Lellouch, E., Bézard, B., Moses, J. I., Davis, G. R., Drossart, P., Feuchtgruber, H., Bergin, E. A., Moreno, R., Encrenaz, T., 2002. The Origin of Water Vapor and Carbon Dioxide in Jupiter's Stratosphere. Icarus 159, 112–131.

Lellouch, E., Moreno, R., Paubert, G., 2005. A dual origin for Neptune's carbon monoxide? Astronomy and Astrophysics 430, L37–L40.

Levison, H. F., Duncan, M. J., Zahnle, K., Holman, M., Dones, L., 2000. NOTE: Planetary Impact Rates from Ecliptic Comets. Icarus 143, 415–420.

Lewis, S. R., Collins, M., Read, P. L., Forget, F., Hourdin, F., Fournier, R., Hourdin, C., Talagrand, O., Huot, J.-P., 1999. A climate database for Mars. Journal of Geophysical Research 104, 24177–24194.

Lissauer, J. J., 1993. Planet formation. Annual Review of Astronomy and Astrophysics 31, 129–174.

Lissauer, J. J., 2005. Formation of the Outer Planets. Space Science Reviews 116, 11–24.

Lodders, K., Fegley, Jr., B., 1994. The origin of carbon monoxide in Neptunes's atmosphere. Icarus 112, 368–375.

Marten, A., Gautier, D., Owen, T., Sanders, D. B., Matthews, H. E., Atreya, S. K., Tilanus, R. P. J., Deane, J. R., 1993. First observations of CO and HCN on Neptune and Uranus at millimeter wavelengths and the implications for atmospheric chemistry. The Astrophysical Journal 406, 285–297.

Melnick, G., Russell, R. W., Gosnell, T. R., Harwit, M., 1983. Spectrophotometry of Saturn and its rings from 60 to 180 microns. Icarus 53, 310–318.

Moreno, R., Marten, A., Matthews, H. E., Biraud, Y., 2003. Long-term evolution of CO, CS and HCN in Jupiter after the impacts of comet Shoemaker-Levy 9. Planetary and Space Science 51, 591–611.

Moses, J. I., Bézard, B., Lellouch, E., Gladstone, G. R., Feuchtgruber, H., Allen, M., 2000a. Photochemistry of Saturn's Atmosphere. I. Hydrocarbon Chemistry and Comparisons with ISO Observations. Icarus 143, 244–298.

Moses, J. I., Lellouch, E., Bézard, B., Gladstone, G. R., Feuchtgruber, H., Allen, M., 2000b. Photochemistry of Saturn's Atmosphere. II. Effects of an Influx of External Oxygen. Icarus 145, 166–202.

Noll, K. S., Knacke, R. F., Geballe, T. R., Tokunaga, A. T., 1986. Detection of carbon monoxide in Saturn. The Astrophysical Journal Letters 309, L91–L94.

Noll, K. S., Larson, H. P., 1991. The spectrum of Saturn from 1990 to 2230/cm - Abundances of AsH3, CH3D, CO, GeH4, NH3, and PH3. Icarus 89, 168–189.

Ollivier, J. L., Dobrijévic, M., Parisot, J. P., 2000. New photochemical model of Saturn's atmosphere. Planetary and Space Science 48, 699–716.

Owen, T., Encrenaz, T., 2006. Compositional constraints on giant planet formation. Planetary and Space Science 54, 1188–1196.

Owen, T., Mahaffy, P., Niemann, H. B., Atreya, S., Donahue, T., Bar-Nun, A., de Pater, I., 1999. A low-temperature origin for the planetesimals that formed Jupiter. Nature 402, 269–270.

Prangé, R., Fouchet, T., Courtin, R., Connerney, J. E. P., McConnell, J. C., 2006. Latitudinal variation of Saturn photochemistry deduced from spatially-resolved ultraviolet spectra. Icarus 180, 379–392.

Prinn, R. G., Barshay, S. S., 1977. Carbon monoxide on Jupiter and implications for atmospheric convection. Science 198, 1031–1034.

Rosenqvist, J., Lellouch, E., Romani, P. N., Paubert, G., Encrenaz, T., 1992. Millimeter-wave observations of Saturn, Uranus, and Neptune - CO and HCN on Neptune. The Astrophysical Journal Letters 392, L99–L102.

Roulston, M. S., Ahrens, T. J., 1997. Impact Mechanics and Frequency of SL9-Type Events on Jupiter. Icarus 126, 138–147.

Smith, H., Buckle, J., Hills, R., Bell, G., Richer, J., Curtis, E., Withington, S., Leech, J., Williamson, R., Dent, W., Hastings, P., Redman, R., Wooff, B., Yeung, K., Friberg, P., Walther, C., Kackley, R., Jenness, T., Tilanus, R., Dempsey, J., Kroug, M., Zijlstra, T., Klapwijk, T. M., 2008. HARP: a sub-millimetre heterodyne array receiver operating on the James Clerk Maxwell Telescope. In: Society of Photo-Optical Instrumentation Engineers (SPIE) Conference Series. Vol. 7020 of Society of Photo-Optical Instrumentation Engineers (SPIE) Conference Series.

Ulich, B. L., 1981. Millimeter-wavelength continuum calibration sources. The Astronomical Journal 86, 1619–1626.

Visscher, C., Fegley, B. J., 2005. Chemical Constraints on the Water and Total Oxygen Abundances in the Deep Atmosphere of Saturn. The Astrophysical Journal 623, 1221–1227.

Wright, E. L., 1976. Recalibration of the far-infrared brightness temperatures of the planets. The Astrophysical Journal 210, 250–253.

Yung, Y. L., Drew, W. A., Pinto, J. P., Friedl, R. R., 1988. Estimation of the reaction rate for the formation of CH3O from H + H2CO - Implications for chemistry in the solar system. Icarus 73, 516–526.

Zahnle, K., 1996. Dynamics and chemistry of SL9 plumes. In: Noll, K. S.,

Weaver, H. A., Feldman, P. D. (Eds.), IAU Colloq. 156: The Collision of Comet Shoemaker-Levy 9 and Jupiter. pp. 183–212.

Zahnle, K., Schenk, P., Levison, H., Dones, L., 2003. Cratering rates in the outer Solar System. Icarus 163, 263–289.